# Frictional Energy Dissipation in a Rough Hertzian Contact

**D. Dini**[1]
Department of Mechanical Engineering,
Imperial College London,
South Kensington Campus,
SW7 2AZ, London, UK
e-mail: d.dini@imperial.ac.uk

**D. A. Hills**
Department of Engineering Science,
University of Oxford,
Parks Road,
OX1 3PJ, Oxford, UK

*The interfacial contact pressure and shear traction distributions are found for a sphere pressed onto an elastically similar half-space whose surface is populated by a uniform array of spherical asperities, when the normal load is constant and an oscillatory shear, less than that needed to cause sliding, is imposed. Details of the load history suffered by asperities in an outer sliding annulus and an inner disk, where they experience partial slip, are found, together with the effects of the roughness on the overall tangential compliance and the frictional energy losses. It is shown that for the example combination of parameters chosen, under light shear loads, the rough contact absorbs less energy than a smooth one subject to the same loading history, but that for larger shearing forces the reverse is true.* [DOI: 10.1115/1.3063697]

*Keywords: Hertzian contact, rough surface, pressure distribution, tangential compliance, partial slip*

## 1 Introduction

A topographically smooth incomplete contact, such as a Hertzian contact (Fig. 1(*a*)), will dissipate energy by frictional hysteresis when it is subjected to a constant normal load and oscillatory tangential shear. The details of the mechanism underlying this phenomenon have been known for over 60 years, since the pioneering solution of Cattaneo [1], rediscovered about 10 years later by Mindlin [2]. Mindlin went on to refine the solution for various loading histories [3,4], and a very comprehensive summary of this piece of work was provided by Deresiewicz [5]. It has proved extremely helpful in understanding the performance of many problems in so-called "partial slip," where fretting damage occurs [6]. Although the dissipation of energy is, in some ways, a phenomenon to be avoided, because it leads to surface damage, it is, at the same time, useful in a range of circumstances where absorption of mechanical energy is desirable, such as a frictional energy damper.

The Cattaneo–Mindlin solution is exact only when applied to the plane form of the contact. This is because, when superposition is used with a three-dimensional problem the transverse component of slip displacement is modified [7], and hence the orthogonality requirement of Coulomb friction is not strictly satisfied. Nevertheless, the solution has been shown to describe well the stick-slip pattern present [8], and the error is usually very small for contacts where the contacting materials have only low or moderate Poisson's ratios [7]. An important generalization of the Cattaneo–Mindlin procedure was developed independently quite recently by Jäger [9] and by Ciavarella [10], who showed that in *any* singly or multiply connected plane contact the Cattaneo procedure for scaling the corrective shear traction will apply and, as with the Cattaneo problem, the technique may be applied with only limited error to a three-dimensional problem.

The design of frictional dampers is currently of considerable interest, particularly in the gas-turbine industry, and the limitations of the classical solution are becoming more apparent in various ways. For example, it is not clear that a classical friction law will continue to apply at very small contact dimensions, and another problem addressed here is the effect of surface roughness. There are many ways in which roughness can be tackled in contact problems, and the approach taken is a very idealized one, intended (a) to expose the general nature of the behavior of partial-slip contacts in the presence of imperfections, (b) to give some idea of the different distributions of dissipation present in a rough contact compared with a smooth one, and (c) to reveal the tangential compliance of the contact, together with its hysteresis loop.

The problem we have tackled here is geometrically very simple, and it is shown in Fig. 1(*b*). An axisymmetric problem has been chosen because it means that the absolute values of both normal and tangential compliances can be found, and these terms have no unique definition in a plane analysis. A sphere of radius $R$ is pressed normally by a force $P$ onto a surface consisting of an array of spherical asperities of radius $\rho$ (Fig. 2). The asperities are regularly spaced on a grid composed of equilateral triangles of side $b$, and there is one asperity that is located immediately beneath the center of the sphere. All the asperities are assumed to have the same height in this very simplified model, although it would not affect the behavior of the system if the asperities were present on the surface of the sphere instead. It is simply easier to think of the problem if we display it in this way. Extensions to the problem by allowing the tip radii of the asperities, or their heights, to vary would be very straightforward, following the Greenwood and Tripp model of roughness [11] and no significant change in the formulation would be needed, although, of course, the number of independent variables would increase.

The first step in the calculation is to determine the number of asperities in contact for a given applied load, the load each individual asperity carries, and the resultant contact pressure distribution. This is done by treating each individual contact as a conventional Hertzian contact, and by thinking of each contact as a point force when its effect on other contacts is being found. Clearly this will not be precisely correct if the asperity spacing is not much bigger than an individual contact disk, but it will improve in quality as the sparseness of the asperity positions, relative to the individual contact diameters, increases. The advantage of this idealization is that it means that the resulting family of simultaneous equations to be solved is linear everywhere except on the leading diagonal. Note, though, that there are two levels of approximation in the procedure. The first is in approximating the effect of an individual asperity by a point force, and the second is in assuming that each individual contact responds as an axisymmetric Hertzian contact, so that the details of the influence of any local surface normal displacement gradient are not taken into account, beyond a constant depression. The primary output in this paper, though, is not the effect of normal load but of shear. When once the normal

[1]Corresponding author.

Contributed by the Tribology Division of ASME for publication in the JOURNAL OF TRIBOLOGY. Manuscript received March 19, 2007; final manuscript received November 13, 2008; published online March 3, 2009. Assoc. Editor: Kwangjin Lee.

  

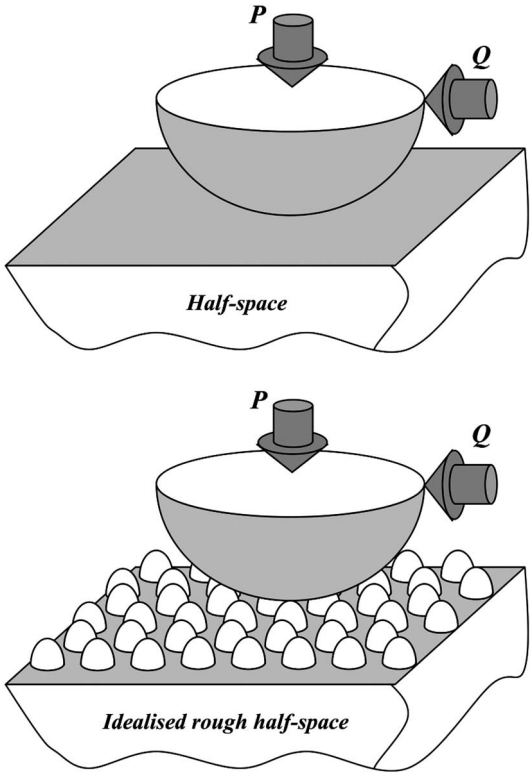


**Fig. 1 (*a*) Hertzian contact problem and (*b*) equivalent idealized rough contact**

contact pressure distribution has been found, use may be made of the Jäger–Ciavarella principle to find the effect of a monotonically increasing shearing force. Most applications of this idea to date have centered on single contacts, but there is no reason why it cannot be applied to multiply connected contacts, as Ciavarella noted [12]. If the coefficient of friction between the contacting surfaces is $f$, and the applied shearing force has been increased to a value $Q(<fP)$, the net shearing traction can be found by taking the slipping distribution $q(x)$ (where $q(x,y)=fp(x,y)$ everywhere) and subtracting from it a scaled form.

Guided by an earlier plane form of the calculation [13], we can infer the general response to be expected: If the contact were smooth, it would consist of a central stick disk surrounded by an annular slip region. In the rough form of the contact, we expect those asperities lying in the macroscopic stick region to be in partial slip, and those in the macroscopic slip region to be in sliding, although the "smooth" stick/slip boundary may not coincide exactly with the boundary between partial-slip/sliding asperities.

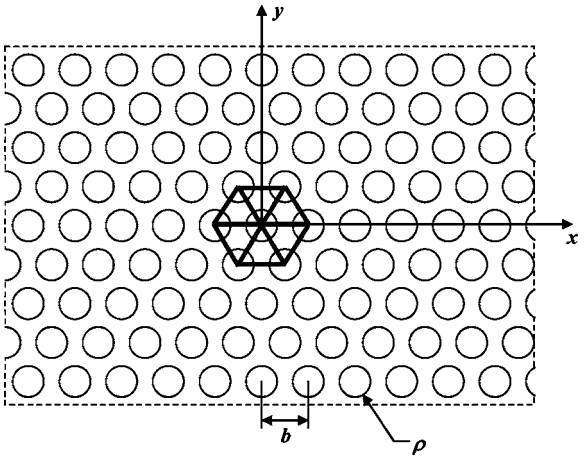


**Fig. 2 "Isometric" asperity distribution**

We will begin by solving the normal contact problem.

## 2 Normal Contact Problem

The standard Hertzian contact solution for a sphere (see Fig. 1(*a*)), of radius $R$, pressed onto the flat surface of an elastically similar half-space by a contact force $P$, gives the approach of two deep points: one within each body $\Delta$ as

$$\Delta^3 = \left(\frac{9}{16E^{*2}R}\right)P^2 \tag{1}$$

where

$$E^* = \frac{E}{2(1-\nu^2)} \tag{2}$$

$E$ is Young's modulus and $\nu$ is Poisson's ratio. Thus, for a solitary Hertzian contact $\Delta \propto P^{2/3}$. We will use this expression to describe the effect of the deformation of an individual asperity *at its own location* [14]. We need now to find the effects of the forces developed at all other asperities on the one under consideration. For the other asperities, it is not necessary to allow for the distributed nature of the contact pressure, and, by appealing to St. Venant's principle, we may idealize their influence as point forces. Thus, the second result we need is the approach of two deep points, one within each body, due to a normal force $P$ applied to the contacting bodies as a point force at the origin of the coordinate system. This is given by

$$\Delta(r) = \frac{P}{\pi E^* r} \tag{3}$$

where

$$r^2 = x^2 + y^2 \tag{4}$$

Consider now the problem depicted in Fig. 1(*b*). First, note that for any individual asperity of radius $\rho$, in contact with the sphere of radius $R$, the relative radius of curvature $R_r$ is

$$\frac{1}{R_r} = \frac{1}{R} + \frac{1}{\rho} = \frac{1}{R}\left(1 + \frac{R}{\rho}\right) \tag{5}$$

For any given asperity $i$, the total surface normal displacement $w_i$, due to both its own contact load and those present at all other asperities, is given by

$$w_i = \left(\frac{9}{16E^{*2}R_r}\right)^{1/3} P_i^{2/3} + \frac{1}{E^*\pi}\sum_{\forall j\neq i}\frac{P_j}{\sqrt{(x_i-x_j)^2+(y_i-y_j)^2}} \tag{6}$$

where the first term represents the effect of the force transmitted by asperity $i$ while the remaining terms, under the summation sign, give the influence of all other asperities. If the two bodies approach each other by an amount $\Delta_0$ the normal approach of a pair of surface points, evaluated at the center of asperity $i$ is given by

$$\Delta(x_i,y_i) = \Delta_0 - \frac{x_i^2+y_i^2}{2R} \tag{7}$$

Within the (initially unknown) contact patch

$$w_i = \Delta(x_i,y_i) \tag{8}$$

which now forms a set of simultaneous equations, while outside the contact patch

$$w_i < \Delta(x_i,y_i) \tag{9}$$

which is the usual inequality for finite separation exterior to the contact. We also require that

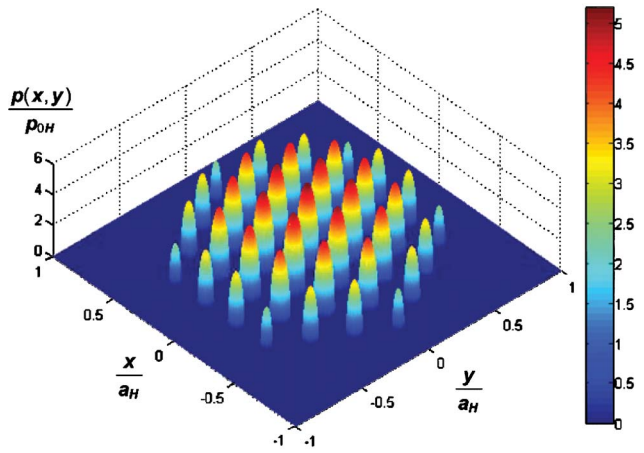


**Fig. 3 Example problem: pressure distribution**

$$P_i > 0, \quad \forall\, i \text{ within the contact}$$
$$\text{(no tensile forces are permitted)} \tag{10}$$

This pair of inequalities, encapsulating the Signorini conditions, is sufficient to define the size of the contact or, here, the specific number of asperities in contact. Lastly, overall equilibrium demands that

$$P = \sum P_i \tag{11}$$

where $P$ is the applied normal load on the macroscopic rough contact.

**2.1 Solution.** As stated earlier, in the example problems examined so far, the asperities are distributed on the half-space using an "isometric" grid (Fig. 2), where the distance between each asperity and its closest neighbors is constant and equal to $b$. We have chosen $\rho/R=0.02$, and $b/R=0.0025$, and an applied load such that 37 asperities are pressed into contact. Of course the contact size is unknown initially, and a first guess may be found from the solution of the equivalent smooth contact problem. In practice we choose a value for the remote approach $\Delta_0/R$ and this is set to $5\times10^{-5}$. The nonlinear simultaneous system of Eqs. (6)–(8) is solved using the conjugate gradient technique implemented within a commercially available nonlinear solver, and is followed by conducting checks for the inequalities in Eqs. (9) and (10). The number of asperities in contact is modified and iteration is carried out until Eqs. (9) and (10) are satisfied. $P$ is then computed using Eq. (11). Once the solution to the rough normal problem has been found, each asperity can be treated as an individual Hertzian contact and the individual contact diameters found. Figure 3 shows the pressure distribution found; the $x-y$ axes represent coordinates in the plane of the contact normalized with respect to the equivalent smooth contact radius $a_H=\sqrt[3]{3PR/4E^*}$, while the altitude denotes the pressure normalized by the maximum Hertzian pressure for the equivalent smooth contact $p_{0H}=\frac{1}{\pi}\sqrt[3]{6PE^{*2}/R^2}$. Not only is the pressure distribution at each asperity in the form of a rotated ellipse, as expected, but the ordinates of the individual asperity contact pressure distributions themselves lie approximately on an overall elliptical form, as might be expected.

## 3 Effect of an Increasing Shear Force

The next step is to determine the influence of the shearing force applied to the macroscopic contact and to find how it is apportioned among the asperities. A direct approach would involve first calculating the tangential compliance of each asperity. This would then permit the individual asperity shear forces to be found, using the concept of a set of springs in parallel. While this is perfectly feasible it is quite tricky to implement, and it is also not necessary. The Ciavarella–Jäger principle demonstrates that, for *any half-plane* contact problem, whether singly or multiply connected, the shearing traction distribution in a partial-slip problem may be found by the following three step procedure.

1. Solve the normal contact problem and corresponding contact pressure distribution.
2. Note that the *sliding* shearing traction distribution is the same function as the contact pressure distribution but scaled by the coefficient of friction.
3. The net shearing traction in partial slip is found by subtracting a further shearing traction distribution. This is scaled in magnitude and extent, compared with the sliding distribution, and corresponds to the contact pressure distribution, which would be present at a lower contact force.

It is this powerful result which obviates the need to conduct the detailed individual contact model procedure described. It is straightforward to find subsequently, for each individual asperity, the shear load supported, and hence the ratio $Q_i/Q$. The Cattaneo–Mindlin problem can hence be solved at the asperity level for the $i$th asperity.

It should be pointed out that if we increase the tangential load $Q$ monotonically from zero, all asperities will initially transmit no shear, and may be thought of as "stuck." As the shearing force is increased, what appears macroscopically as a slip annulus will start to develop from the outside of the contact, and the stick-slip boundary will migrate inwards as the shearing force is applied. Further, those asperities, which are in the macroscopic stick region will themselves exhibit partial slip, while those in the macroscopic slip region, will slide. Therefore, all asperities not near the contact boundary will go into partial slip as the shearing force is applied, and if the shearing force becomes large enough, they will experience a transition to full sliding. Figure 4(*a*) shows the rings on which asperities are centered (labeled A–F, which will be referred to shortly) while Fig. 4(*b*) shows an example distribution of asperity responses, for the particular load $Q/fP=0.5$. Here only six asperities belong to the slip annulus (schematically approximated by the dotted lines) and all the other asperities are still within the macroscopic stick region and therefore are themselves experiencing partial slip. The results are shown in detail in Fig. 5. As expected, there is an outer annulus of sliding asperities and an inner array of asperities, over an apparently adhering disk, which are, in fact, in partial slip, as the magnified view of the central asperity, which is the one exhibiting the smallest tendency to slide, shows. A more quantitative display of the same information is provided in Fig. 6, which shows the shearing traction distribution through the central plane $y=0$. It should be noted that the Cattaneo–Mindlin solution at the single asperity level is recovered and the results obtained using the 2D plane strain equivalent formulation [13] can be easily retrieved. Figure 7(*a*) shows the evolution of the dimensionless shearing force $Q_i/fP_i$ supported on the $i$th asperity, as the overall shearing force $Q/fP$ is increased. The letters A–F refer to the radial position of asperities introduced in Fig. 4(*a*).

We now turn to the tangential displacements at the contact interface. The load-displacement characteristic for partial-slip loading can be expressed as a relationship between the component of the tangential displacement at the $i$th asperity, in the same direction as the applied shear force $\Delta_t^i$, the loading regime $Q_i/fP_i$, and the elastic material constants, and is given by [2]

$$\Delta_t^i = \frac{3(2-\nu)fP_i}{16\mu a_i}\left[1-\left(1-\frac{Q_i}{fP_i}\right)^{2/3}\right] \tag{12}$$

The tangential displacement at each asperity $\Delta_t^i$ increases with overall applied shear (Fig. 7(*b*)). There are six curves, corresponding to rings of asperities A–F (Fig. 4(*a*)) and they are labeled at

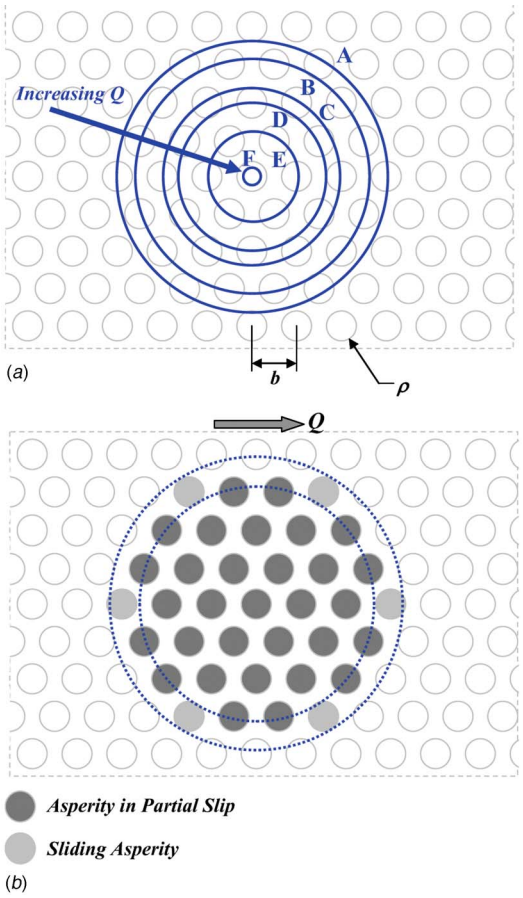


**Fig. 4 A discrete evolution of the stick region as a function of the tangential load *Q*. (*a*) Due to the discrete nature of the problem, the asperities centered on "rings" A–F (central asperity) will enter the slip annulus discontinuously while varying the tangential load *Q* monotonically from 0 to *fP*. (*b*) Example distribution for *Q*/*fP*=0.5: Here only six asperities belong to the slip annulus (schematically approximated by the dotted lines).**

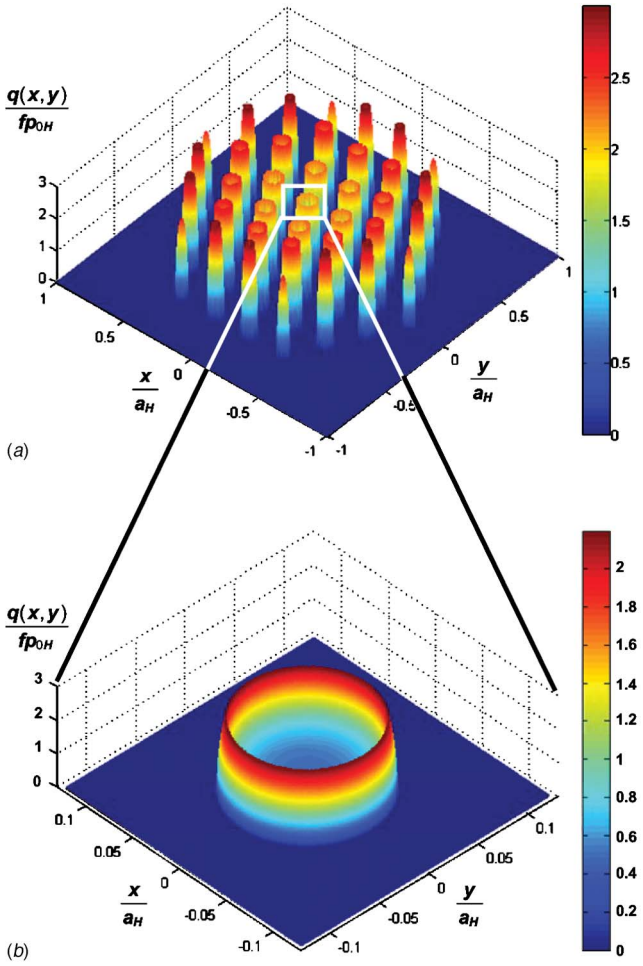


**Fig. 5 Shear traction distribution for *Q*/*fP*=0.5: (*a*) overall and (*b*) localized (central asperity) three-dimensional distributions**

the right-hand side of the plot. The important feature, here, are the "steps" in displacement evident at several points in the curves (and indicated by the black arrows). These are not caused by numerical problems, but they arise as asperities toward the edge of the macroscopic stick region reach the sliding condition and so make the transition to the broadening slip annulus (the progression is also indicated by the letters A–E adjacent to the vertical arrows identifying the ring of asperities entering the slip annulus corresponding to each step, and first used in Fig. 4(*a*)).

We now consider the effect of a cyclic shear force. The computation of the energy dissipated during repeated partial-slip loading cycles requires both the evolution of shear traction and relative tangential displacements to be determined at asperity level. In order to calculate the shear tractions for a varying shear force $Q$, two corrective terms describing the redistribution of shear are required during the unloading and reloading phases. Again this may be treated using the Ciavarella–Jäger principle and the shearing tractions evolving found. The expression for the shearing force at each asperity is now given by the superposition of three terms, with the second and the third contributions scaled in both magnitude and extent.

## 4 Energy Absorption

A very powerful technique was evolved by Mindlin and colleagues [4] for determining the frictional energy expenditure, and hence the formation of hysteresis loops. The most direct way of evaluating frictional losses would, of course, be to look at the shearing tractions present within the contact and to determine the slip displacement experienced during a loading cycle. This would reveal the density of frictional work expended, which could then be integrated over the true contact area. However, the approach is

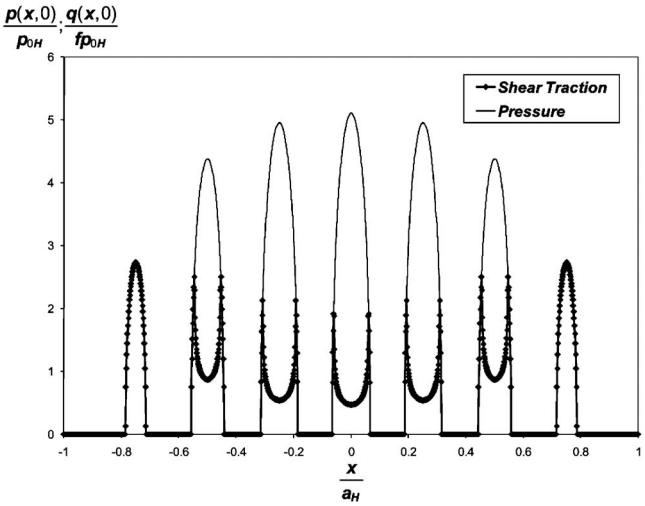


**Fig. 6 Normalized pressure and shear traction distribution for *Q*/*fP*=0.5 and *y*=0**

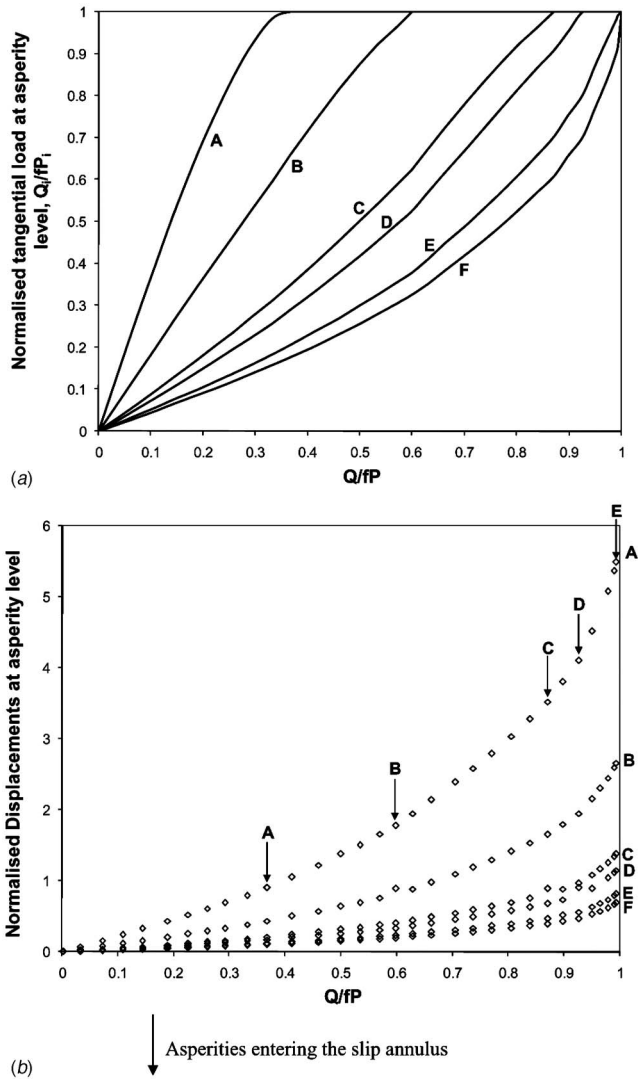


**Fig. 7 Dimensionless (*a*) shearing forces and (*b*) displacements at asperity level as a function of the dimensionless tangential load $Q/fP$**

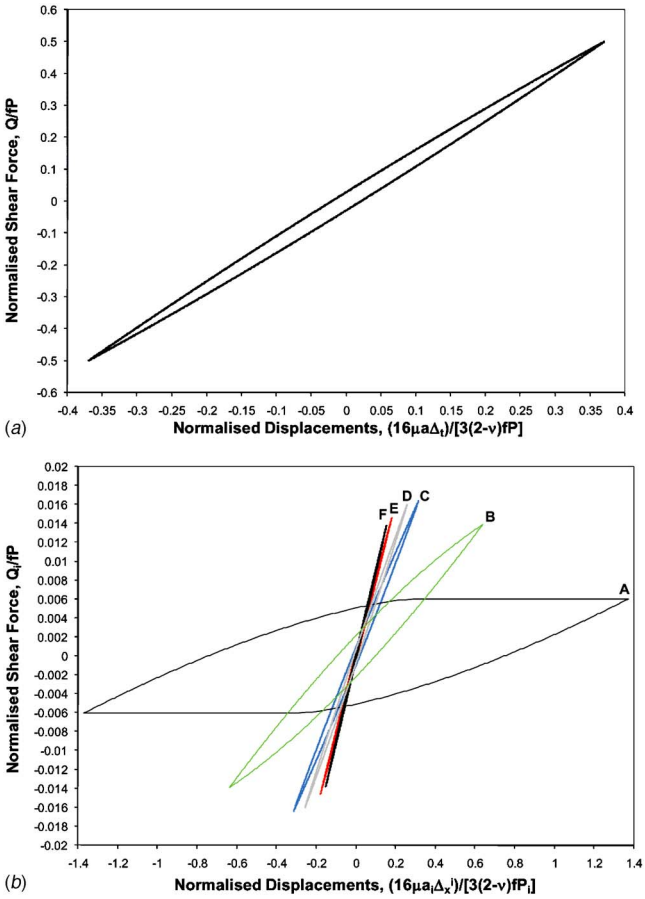


**Fig. 8 Normalized displacements versus normalized shear force loops for $Q^{max}/fP=0.5$: (*a*) smooth equivalent contact and (*b*) asperities**

numerically intensive and tedious, and Mindlin noted that the losses are also manifested in the form of the changing tangential compliance/shearing force hysteresis loops of the contact. By looking at the losses in this way, the need to integrate the effects over the contact area is avoided, and, in this particular case, the economy in computational effort is even greater than in the case of a solitary contact. Details of the calculation are given in Refs. [3,5], and, for a single, topographically smooth Hertzian contact, the hysteresis loop is displayed in Fig. 8(*a*), for reference. During the application of the initial shear, the deep-point tangential displacement $\Delta_t$ is given by

$$\Delta_t = \frac{3(2-\nu)fP}{16\mu a}\left[1-\left(1-\frac{Q}{fP}\right)^{2/3}\right] \tag{13}$$

during loading. During unloading,

$$\Delta_{t,u} = \frac{3(2-\nu)fP}{16\mu a}\left[2\left(1-\frac{Q^{\max}-Q}{2fP}\right)^{2/3}-\left(1-\frac{Q^{\max}}{fP}\right)^{2/3}-1\right] \tag{14}$$

and finally during reloading,

$$\Delta_{t,r} = -\frac{3(2-\nu)fP}{16\mu a}\left[2\left(1-\frac{Q^{\max}+Q}{2fP}\right)^{2/3}-\left(1-\frac{Q^{\max}}{fP}\right)^{2/3}-1\right] \tag{15}$$

The last two equations define the form of the curve in the steady state partial-slip cycle. The resultant energy expenditure can also be found in closed form as reported in Ref. [5].

$$E_f = \frac{9(2-\nu)f^2P^2}{10\mu a}\left[1-\left(1-\frac{Q^{\max}}{fP}\right)^{5/3}-\frac{5Q^{\max}}{6fP}\left[1+\left(1-\frac{Q^{\max}}{fP}\right)^{2/3}\right]\right] \tag{16}$$

Although this technique is very ingenious and can be applied both at the macroscopic scale (for a smooth contact) and at the asperity scale for a rough contact, it cannot be used to determine the work done against friction by those asperities, which are sliding. However, it is still not necessary to carry out an integration of the work over the asperity contact area. Instead, we simply treat each asperity contact as a sliding point force. Care is still needed when calculating the sliding distance, as this is controlled by both the macroscopic contact compliance (which drives the asperity toward sliding) and the compliance of the individual contact (which reduces slightly the distance slid). Details are given in the Appendix.

In Fig. 8(*b*) hysteresis loops are plotted for three individual asperities present on the surface of the example rough macroscopic contact being studied. The normalization is itself now performed at the asperity level, and the evolution of $16\mu a_i\Delta_x^i/3(2$

$-\nu)fP_i$ is plotted as a function of $Q_i/fP$. It should also be noted here that for the asperity in the slip annulus (A), the flat portion of the loop corresponds to saturated values of $Q_i=fP_i$ and $\Delta_x^{i,\max} - \Delta_t^{i,\max}$ represents the maximum relative displacement of the sliding asperities with respect to the stick region. The central asperity, which is the one experiencing the lowest ratio of $Q_i/fP_i$, gives the narrowest loop (F), while those on the rings E–B in Fig. 4 are characterized by slightly wider loops, progressively larger as the asperities approach the slip annulus (see B). However, most striking are the loops for the sliding asperities, which form the extremely broad loops with saturated shearing forces. It is quite clear that, for problems of this kind, the vast majority of the energy is expended in sliding the asperities backward and forward in the slip annulus, while the energy absorbed by those in the macroscopic stick region is small. However, it should be again emphasized that the slip displacement exhibited by the partial-slip asperities does control the overall tangential compliance of the configuration, and therefore the magnitude of the slip displacement of those asperities, which slide. They therefore effectively control the "width" of the sliding asperity loops, in the sense of the width of the parallelogram, which constitutes the work associated with sliding. Note that the "barreled" sides of the loop remain the same for any sliding asperity, regardless of the sliding displacement and are, in fact, of exactly the same shape as the full hysteresis loop of an asperity about to undergo incipient sliding.

## 5 Discussion of Results

For the example geometry and for a fully reversing shearing force, oscillating between $Q^{\max}$ and $-Q^{\max}$ the energy absorbed by the contact as a function of the magnitude of $Q^{\max}/fP$ is shown in Fig. 9(*a*). This clearly shows how the hysteresis losses, while remaining a monotonically increasing function of the dimensionless shearing force range, exhibit distinct steps in behavior as the force range is increased. Also shown on the same graph is the energy absorbed by a perfectly smooth spherical contact, devoid of asperities, experiencing the same shearing force history. The nondimensionalization of the energy expenditure used here is $10\mu a E_f/9(2-\nu)f^2P^2$, plotted against $Q^{\max}/fP$. When there are relatively few asperities sliding, and the contact (as shown at a larger scale in Fig. 9(*b*)) is in a near full-stick condition, the rough contact absorbs less energy than the smooth one. However, at a ratio of $Q^{\max}/fP$ of about 0.37 this property is reversed, and the rough contact absorbs more energy. The gap between the two solutions shows a very complicated trend, and this feature can be traced back to the effect of asperities moving discretely from the bulk stick to the bulk slip region, described in some detail in Sec. 4. When plotted in this form, though, the effect is much more pronounced.

## 6 Conclusion

The stick-slip regime prevalent in an idealized rough axisymmetric Hertzian contact, subject to a constant normal load and an oscillatory shear, has been found. The details of frictional dissipation at the asperity level have been revealed, and the hysteresis loop found both at the asperity level and at the aggregate level of the macroscopic contact. It has been shown that the energy absorbed depends on the range of shearing force. For the example case studied, a very lightly loaded smooth contact absorbs very slightly more than the rough one, but when the shearing force exceeds about 37% of the sliding value, the rough contact starts to absorb more, and the difference increases as the sliding condition is approached.

Clearly there are many combinations of parameters, which can be varied here, and the function of this paper has simply been to display the method and show its effectiveness. Natural extensions are to vary the degree of shear load reversal, so that frictional shakedown is possible, together with a more realistic roughness model allowing for a variation in asperity heights and tip radii. This will be undertaken in due course.

During preparation of this paper two articles have appeared (in electronic form) on related topics. The first, by Kasarekar et al. [15], seeks to address wear of rough surfaces in partial slip and uses a formulation based on a Fourier representation of the surface. The second, by Luan and Robbins [16] follows previous studies by the same authors on comparing continuum contact mechanics to atomistic simulations. It should be noted that some of the results obtained in terms of atomic interactions can be explained at the continuum level using the approach described here.


## Acknowledgment

The authors would like to thank one of the anonymous referees for his/her helpful comments, which have greatly contributed to the improvement of the manuscript. We acknowledge the support of the EPSRC under the Grant No. EP/E057985/1. D.D. would also like to thank the Royal Swedish Academy of Engineering Sciences for the support received through the Jacob Wallenberg Research Foundation Grant 2007.


## Appendix: Surface Relative Tangential Slip Displacement

The relative displacement between the adhered macroscopic contact area and the asperities belonging to the slip annulus, when they undergo gross sliding, is required to compute the energy expenditure corresponding to those asperities. Therefore, the contribution of every asperity to the relative surface displacement in the tangential ($x$) direction needs to be taken into account. Once the shear tractions at the interface have been computed at each asperity, the tangential displacement can be computed following the formulation given in Ref. [17]. For a fully reversing cycle, the relative tangential displacement at the $i$th asperity at the maximum load is given by

$$\Delta_s^i = \left| \sum_{\forall j} u_x^{i,j}(r_{i,j}(x_i,y_i)) - \Delta_{\text{adhered}} \right| \tag{A1}$$

where

$$u_x^{i,j}(r_{i,j}(x_i,y_i)) = u_{x,fp}^{i,j} - u_{x,q}^{i,j} \tag{A2}$$

and

$$u_{x,fp}^{i,j} = \begin{cases} \dfrac{\pi a_j q_{0j}}{32\mu}\left[4(2-\nu) - (4-\nu)\left(\dfrac{(y_i-y_j)}{a_j}\right)^2 - (4-3\nu)\left(\dfrac{(x_i-x_j)}{a_j}\right)^2\right], & r_{i,j}(x_i,y_i) \le a_j \\ \dfrac{\pi a_j q_{0j}}{32\mu}\left[(2-\nu)\left[D2_{i,j}\sin^{-1}(D0_{i,j}) + \dfrac{D3_{i,j}}{D0_{i,j}}\right] + \dfrac{1}{2}\nu D1_{i,j}\left[\left(\dfrac{1}{D0_{i,j}}\right)^2 \sin^{-1}(D0_{i,j}) + D0_{i,j}D3_{i,j}D2_{i,j}\right]\right], & r_{i,j}(x_i,y_i) > a_j \end{cases} \tag{A3}$$

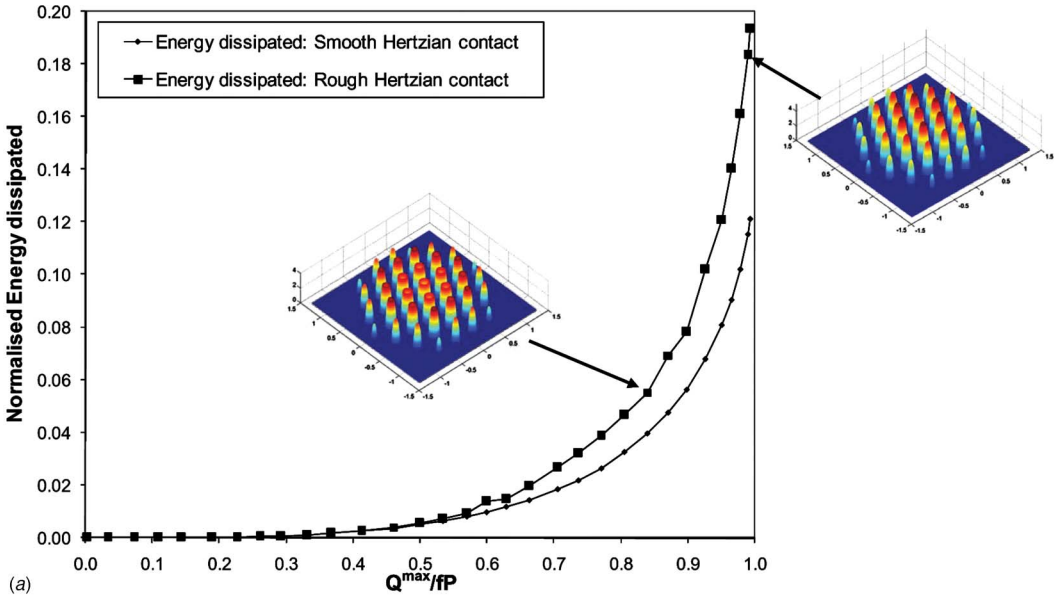


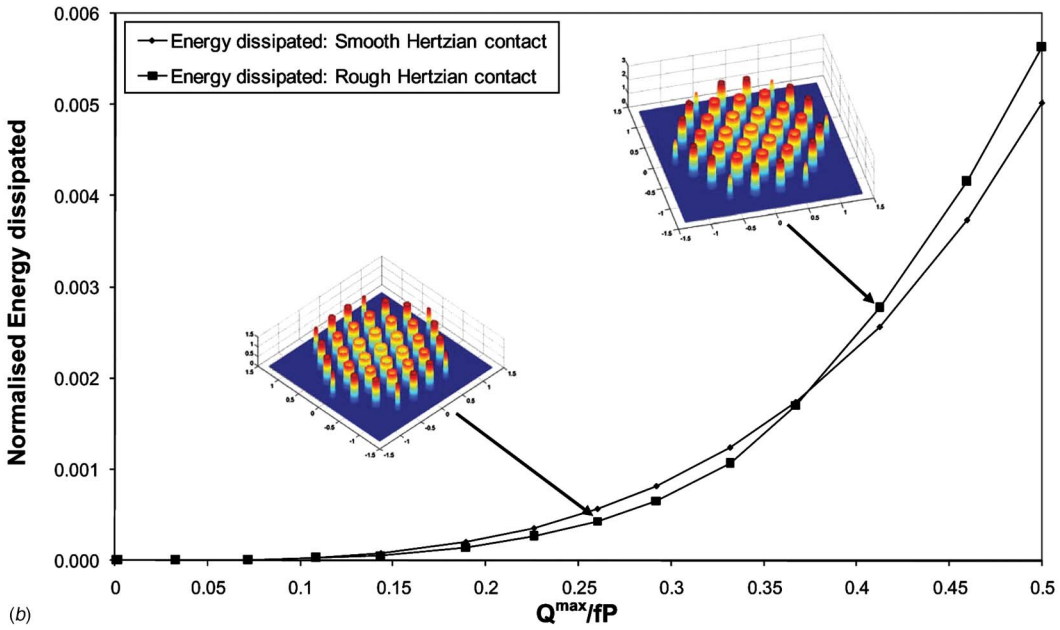


**Fig. 9** (*a*) **Normalized frictional energy dissipated as a function of the macroscopic normalized shear force. Two examples of shear traction distributions corresponding to two loading conditions are also displayed as an inset to the figure.** (*b*) **Zoom-in of the plot in Fig. 9(*a*) at low levels of normalized tangential forces. Two examples of shear traction distributions corresponding to two loading conditions are also displayed as an inset to the figure.**

$$u_{x,q}^{i,j} = \begin{cases} \dfrac{\pi \dfrac{c_j^2}{a_j} q_{0j}}{32\mu}\left[4(2-\nu) - (4-\nu)\left(\dfrac{(y_i - y_j)}{c_j}\right)^2 - (4-3\nu)\left(\dfrac{(x_i - x_j)}{c_j}\right)^2\right], & r_{i,j}(x_i, y_i) \le c_j \\ \dfrac{\pi \dfrac{c_j^2}{a_j} q_{0j}}{32\mu}\left[(2-\nu)\left[D2c_{i,j}\sin^{-1}(D0c_{i,j}) + \dfrac{D3c_{i,j}}{D0c_{i,j}}\right] + \dfrac{1}{2}\nu D1c_{i,j}\left[\left(\dfrac{1}{D0c_{i,j}}\right)^2 \sin^{-1}(D0c_{i,j}) + D0c_{i,j}D3c_{i,j}D2_{i,j}\right]\right], & r_{i,j}(x_i, y_i) > c_j \end{cases} \tag{A4}$$

$$q_{0j} = f p_{0j} = \frac{f}{\pi}\sqrt[3]{\frac{6E^{*2}P_j}{R_r^2}} \tag{A5}$$

$$c_j = a_j \sqrt[3]{1 - \frac{Q_j}{fP_j}} \tag{A6}$$

$$r_{i,j}(x_i,x_j) = \sqrt{(x_i - x_j)^2 + (y_i - y_j)^2} \tag{A7}$$

$$D0_{i,j} = \frac{a_j}{r_{i,j}(x,x_j)} \tag{A8}$$

$$D0c_{i,j} = \frac{c_j}{r_{i,j}(x,x_j)} \tag{A9}$$

$$D1_{i,j} = [(x_i - x_j)^2 - (y_i - y_j)^2] \tag{A10}$$

$$D2_{i,j} = \left[2 - \left(\frac{r_{i,j}(x_i,x_j)}{a_j}\right)^2\right] \tag{A11}$$

$$D2c_{i,j} = \left[2 - \left(\frac{r_{i,j}(x_i,x_j)}{c_j}\right)^2\right] \tag{A12}$$

$$D3_{i,j} = \sqrt{1 - \left(\frac{a_j}{r_{i,j}(x_i,x_j)}\right)^2} \tag{A13}$$

$$D3c_{i,j} = \sqrt{1 - \left(\frac{c_j}{r_{i,j}(x_i,x_j)}\right)^2} \tag{A14}$$

Here $\Delta_{\text{adhered}}$ is the (constant) displacement of the asperities belonging to the stick region, induced by the shear traction distributions at the asperity level.

$$\Delta_{\text{adhered}} = \Delta_s^i, \quad \forall\,(x_i,y_i) \subset Q_i \leq fP_i \tag{A15}$$

The total displacement at the asperity level along the direction of application of the load can hence be computed as

$$\Delta_x^i = \Delta_t^i + \Delta_s^i \tag{A16}$$

## References


[1] Cattaneo, C., 1938, "Sul Contatto di Due Corpi Elasti: Distribuzione Locale degli Sforzi," Accademia Nazionale dei Lincei, Rendiconti, **27**(6), pp. 342–348.

[2] Mindlin, R. D., 1949, "Compliance of Elastic Bodies in Contact," ASME J. Appl. Mech., **16**, pp. 259–268.

[3] Mindlin, R. D., and Deresiewicz, H., 1953, "Elastic Spheres in Contact Under Varying Oblique Forces," ASME J. Appl. Mech., **20**, pp. 327–344.

[4] 1989, *The Collected Papers of Raymond D. Mindlin*, H. Deresiewicz, M. P. Bieniek and F. L. DiMagio, eds., Springer, New York, Vols. 1 and 2.

[5] Deresiewicz, H., 1974, "Bodies in Contact With Applications to Granular Media," *R. D. Mindlin and Applied Mechanics*, G. Herrmann, ed., Pergamon, Oxford, UK.

[6] Nowell, D., Dini, D., and Hills, D. A., 2006, "Recent Developments in the Understanding of Fretting Fatigue," Eng. Fract. Mech., **73**(2), pp. 207–222.

[7] Munisamy, R. L., Hills, D. A., and Nowell, D., 1994, "Static Axisymmetric Hertzian Contacts Subject to Shearing Forces," ASME J. Appl. Mech., **61**(2), pp. 278–283.

[8] O'Connor, J. J., and Johnson, K. L., 1963, "The Role of Surface Asperities in Transmitting Tangential Forces Between Metals," Wear, **6**, pp. 118–139.

[9] Jäger, J., 1998, "A New Principle in Contact Mechanics," ASME J. Tribol., **120**(4), pp. 677–684.

[10] Ciavarella, M., 1998, "The Generalized Cattaneo Partial Slip Plane Contact Problem. I: Theory," Int. J. Solids Struct., **35**(18), pp. 2349–2362.

[11] Greenwood, J. A., and Tripp, J. H., 1967, "The Elastic Contact of Rough Spheres," ASME J. Appl. Mech., **34**, pp. 153–159.

[12] Ciavarella, M., 1998, "The Generalized Cattaneo Partial Slip Plane Contact Problem. II: Examples," Int. J. Solids Struct., **35**(18), pp. 2363–2378.

[13] Ciavarella, M., Hills, D. A., and Moobola, R., 1999, "Analysis of Plane, Rough Contacts, Subject to a Shearing Force," Int. J. Mech. Sci., **41**(1), pp. 107–120.

[14] Hills, D. A., and Nowell, D., 1994, *Mechanics of Fretting Fatigue*, Kluwer Academic, Dordrecht, The Netherlands.

[15] Kasarekar, A. T., Bolander, N. W., Sadeghi, F., and Tseregounis, S., 2007, "Modeling of Fretting Wear Evolution in Rough Circular Contacts in Partial Slip," Int. J. Mech. Sci., **49**(6), pp. 690–703.

[16] Luan, B., and Robbins, M. O., 2006, "Contact of Single Asperities With Varying Adhesion: Comparing Continuum Mechanics to Atomistic Simulations," Phys. Rev. E, **74**, p. 026111.

[17] Johnson, K. L., 1985, *Contact Mechanics*, Cambridge University Press, Cambridge, UK.